

# Relativistic energy-momentum tensor distributions in a polarized nucleon

Ho-Yeon Won<sup>1,\*</sup> and Cédric Lorce<sup>1,†</sup>

<sup>1</sup>*CPHT, CNRS, École Polytechnique, Institut Polytechnique de Paris, 91120 Palaiseau, France*

(Dated: March 11, 2025)

We study in detail the relativistic distributions of energy, longitudinal momentum, longitudinal energy flux, and longitudinal thrust inside nucleons based on the quantum phase-space formalism. Similar to recent studies on the electromagnetic current, we include the effects of the nucleon polarization and show that the latter are essential for understanding how the Breit frame distributions transform under a longitudinal Lorentz boost. We also explicitly demonstrate that, in the infinite-momentum frame, these distributions allow one to recover not only the “good” but also the “bad” components of the light-front energy-momentum tensor distributions.

## I. INTRODUCTION

A critical challenge in hadronic physics is to unravel the internal structure of the nucleons. It is also one of the key questions that the future Electron-Ion Collider (EIC) experiments [1, 2] in the USA aims to address, namely “*How are partons inside the nucleon distributed in both momentum and position space?*”. The energy-momentum tensor (EMT) emerged as a promising candidate for addressing these questions in the framework of quantum chromodynamics (QCD). It plays a crucial role in encoding information about the internal structure, including the mass, spin, and mechanical properties of the nucleon, see [3, 4] for recent reviews on both theoretical and experimental aspects.

Similar to the electromagnetic current, the matrix elements of the EMT are described in terms of form factors (FFs), which are Lorentz-invariant functions encoding the spatial extension and structure of the nucleon. These EMT FFs can be accessed indirectly through generalized parton distributions [5, 6]. A chiral decomposition of the EMT motivated the introduction of the P-odd partner of the EMT, which also allows the study of the spin-orbit correlations [7–10]. In addition, the relation between the EMT and transverse-momentum dependent parton distributions has recently been explored in [11].

Spatial distributions are defined via a Fourier transform of the matrix elements evaluated in some particular frame. Three-dimensional EMT distributions in the Breit frame (BF) have been introduced in [12]. BF distributions are known to be plagued by relativistic recoil corrections which spoil their interpretation as genuine densities. Alternatively, the light-front (LF) formalism allows one to define genuine two-dimensional relativistic densities in the Drell-Yan frame (DYF) [13–16]. The LF EMT distributions for an unpolarized nucleon with vanishing transverse momentum have been introduced in [17] and shown to coincide with the EMT distributions in the infinite-momentum frame (IMF). These LF distribu-

tions have then been generalized to arbitrary values of the nucleon transverse momentum [18]. As a result of the Galilean symmetry of the LF formalism in the transverse plane, the intrinsic LF distributions simply coincide with those defined at vanishing transverse momentum. An annoying feature of this formalism is that transverse nucleon polarization induces distortions in e.g. the LF charge [19] and LF momentum [20] distributions.

An interpolation between the BF and IMF EMT distributions can be defined within a phase-space approach, where the relativistic distributions are regarded only as quasi-densities [17]. However, only unpolarized distributions were considered and a complete understanding of how BF EMT distributions evolve into IMF EMT distribution could not be reached. Recent studies on the frame dependence of the electromagnetic charge and current distributions [21–23] clarified the situation and revealed that the Wigner spin rotation plays a crucial role in this matter.

In this work, we extend the analysis of [17] by including the nucleon polarization. The paper is organized as follows. In Sec. II, we remind the parametrization of the EMT matrix elements and some of its key properties. Then, in Sec. III, we review the definition of the relativistic spatial distributions within the quantum phase-space approach, and we analyze the distributions of energy, longitudinal momentum, longitudinal energy flux, and longitudinal thrust for both unpolarized and transversely polarized nucleons. Switching to the LF components, we show in Sec. IV that these distributions coincide in IMF limit with the LF ones. After a summary of our results, we added three appendices where we (A) discuss some details regarding the value of the dipole mass used for quark spin FF, (B) present an alternative parametrization of the EMT matrix elements directly in terms of the BF multipole FFs, and (C) show additional plots for the longitudinal momentum and longitudinal thrust distributions.

\*E-mail: hoyeon.won@polytechnique.edu

†E-mail: cedric.lorce@polytechnique.edu

## II. MATRIX ELEMENTS OF THE ENERGY-MOMENTUM TENSOR

As a result of the Poincaré symmetry, the matrix elements of the local gauge-invariant and asymmetric EMT

---


$$\begin{aligned} \langle p', s' | \hat{T}_a^{\mu\nu}(0) | p, s \rangle = \bar{u}(p', s') & \left[ \frac{P^{\{\mu\gamma\nu\}}}{2} A_a(Q^2) + \frac{\Delta^\mu \Delta^\nu - g^{\mu\nu} \Delta^2}{4M} D_a(Q^2) + M g^{\mu\nu} \bar{C}_a(Q^2) \right. \\ & \left. + \frac{i P^{\{\mu\sigma\nu\}\rho} \Delta_\rho}{4M} B_a(Q^2) - \frac{i P^{[\mu\sigma\nu]\rho} \Delta_\rho}{2M} S_a(Q^2) \right] u(p, s), \end{aligned} \quad (1)$$


---

where the subscript  $a$  stands for a specific type of constituent, namely quark or gluon. For simplicity, we use the notations  $a^{\{\mu b\nu\}} = a^\mu b^\nu + a^\nu b^\mu$  and  $a^{[\mu b\nu]} = a^\mu b^\nu - a^\nu b^\mu$ . The four-momentum eigenstates are normalized as  $\langle p', s' | p, s \rangle = 2P^0 (2\pi)^3 \delta^{(3)}(\mathbf{p}' - \mathbf{p}) \delta_{s's}$  with the canonical spin polarizations  $s', s$ .  $P = (p' + p)/2$  and  $\Delta = p' - p$  denote the average momentum and momentum transfer, respectively. Since  $\Delta$  is a spacelike four-vector, we use for convenience the Lorentz-invariant variable  $Q^2 = -\Delta^2$ .

The spin FF for quarks  $S_q$  is related to the axial-vector FF via the QCD equation of motion [24–26], while it vanishes for gluons

$$S_q(Q^2) = \frac{1}{2} G_A^q(Q^2), \quad S_G(Q^2) = 0. \quad (2)$$

The total EMT FFs are obtained by summing over the quark and gluon contributions

$$\begin{aligned} \mathcal{F}(Q^2) &= \mathcal{F}_q(Q^2) + \mathcal{F}_G(Q^2), \\ \mathcal{F}_q(Q^2) &= \sum_{f=u,d,\dots} \mathcal{F}_f(Q^2), \end{aligned} \quad (3)$$

where  $\mathcal{F} = A, B, D, \bar{C}, S$ . Since the symmetrized total EMT is not renormalized [27], the total FFs factors  $A$ ,  $B$ ,  $D$ , and  $\bar{C}$  are scheme and scale independent. The conservation of total linear and angular momenta imply in addition the following constraints [24, 28–30]

$$A(0) = 1, \quad B(0) = 0, \quad \bar{C}(Q^2) = 0. \quad (4)$$

In contrast,  $D(0)$  is not constrained by Poincaré symmetry but is conjectured to be negative in hadrons based on stability arguments [31, 32]. The vanishing of the total  $\bar{C}$  FF follows directly from the EMT conservation  $\partial_\mu \hat{T}^{\mu\nu} = 0$ . This does not mean, however, that the individual quark and gluon contributions  $\bar{C}_a(Q^2)$  are also zero.

In the present work, we will adopt a simple multipole Ansatz for the EMT FFs to illustrate our results

$$\mathcal{F}_a(Q^2) = \frac{\mathcal{F}_a(0)}{(1 + Q^2/\Lambda_{\mathcal{F}_a}^2)^{n_F}}. \quad (5)$$

current [24] can be parametrized for a spin-1/2 target with mass  $M$  [5, 25] in terms of five EMT FFs as follows:

Such a form is supported, e.g., by calculations in the chiral quark-soliton model [33–37]. The parameters of the multipole Ansatz for  $A$ ,  $B$ ,  $\bar{C}$ , and  $D$  FFs are given in Ref. [17]. Regarding the quark spin FF, we will use the dipole mass  $\Lambda_{S_q} = 1.00$  GeV and the normalization  $S_q(0) = \frac{1}{2} g_A^0 = 0.17$ . Changing the value of this dipole mass strongly affects the sign of the OAM FF, the nucleon spin polarization, and the dipole structure of the longitudinal OAM distribution in the BF, see Appendix A for a detailed discussion.

## III. DISTRIBUTIONS IN ELASTIC FRAME

A class of Lorentz frames, called the elastic frame (EF), has been introduced in Ref. [26] to study the relativistic spatial distributions of total angular momentum (TAM), orbital angular momentum (OAM), and spin inside the nucleon. The formalism developed into a relativistic phase-space picture [38] and was then used to study the spatial distributions of the EMT [17], the electromagnetic current [21–23, 39–42], and the axial-vector current [43, 44], along with their dependence on the hadron momentum.

Whereas the former EMT study [17] was limited to an unpolarized nucleon target, we include in the present work the contributions from the nucleon polarization. As demonstrated in the cases of the electromagnetic [23] and axial-vector [43] currents, the latter is essential to a complete understanding of the dependence of the spatial distribution on the nucleon momentum.

## A. General expressions

Following the phase-space formalism, we can express the 2D spatial distributions of the EMT in the EF as

$$\begin{aligned} T_a^{\mu\nu}(\mathbf{b}_\perp, P_z; s', s) &= \int dr_z \left\langle \hat{T}_a^{\mu\nu}(\mathbf{r}) \right\rangle_{\mathbf{R}, \mathbf{P}=P_z \hat{e}_z; s', s} \\ &= \int \frac{d^2 \Delta_\perp}{(2\pi)^2} e^{-i \Delta_\perp \cdot \mathbf{b}_\perp} \left. \frac{\langle p', s' | \hat{T}_a^{\mu\nu}(0) | p, s \rangle}{2P^0} \right|_{\text{EF}}, \end{aligned} \quad (6)$$

where the spatial axes are chosen so that the average momentum takes the form  $\mathbf{P} = (\mathbf{0}_\perp, P_z)$ . The impact parameter coordinates,  $\mathbf{b}_\perp = (\mathbf{r}_\perp - \mathbf{R}_\perp, 0)$ , represent the transverse position relative to the center of the system. The integral over the longitudinal component in position space enforces  $\Delta_z = 0$  and hence the elastic condition, i.e. zero energy transfer  $\Delta^0 = \Delta \cdot \mathbf{P}/P^0 = 0$ . As a result, the 2D distributions in the EF remain time-independent. Given that  $P^2 = M^2(1 + \tau)$  with  $\tau = Q^2/4M^2$ , the average energy in the EF is  $P^0 = p^0 = \sqrt{P_z^2 + M^2(1 + \tau)}$ . In the limit  $P_z \rightarrow 0$ , the EF coincides with the transverse BF. Conversely, as  $P_z \rightarrow \infty$ , the EF approaches the IMF.

If we denote by  $\Lambda$  the boost from the BF momentum  $p_{\text{BF}}$  to some momentum  $p$ , the EMT matrix elements transform according to [45, 46]

$$\begin{aligned} &\langle p', s' | \hat{T}_a^{\mu\nu}(0) | p, s \rangle \\ &= \sum_{s'_{\text{BF}}, s_{\text{BF}}} D_{s'_{\text{BF}} s_{\text{BF}}}^{(j)}(p_{\text{BF}}, \Lambda) D_{s'_{\text{BF}} s_{\text{BF}}}^{*(j)}(p'_{\text{BF}}, \Lambda) \\ &\quad \times \Lambda^\mu_\alpha \Lambda^\nu_\beta \langle p'_{\text{BF}}, s'_{\text{BF}} | \hat{T}_a^{\alpha\beta}(0) | p_{\text{BF}}, s_{\text{BF}} \rangle, \end{aligned} \quad (7)$$

where  $D^{(j)}$  is the Wigner rotation matrix for spin- $j$  particles. For spin-1/2 particles, the latter can be written as follows:

$$D_{s' s}^{(1/2)}(p, \Lambda) = \cos \frac{\theta}{2} \delta_{s' s} + i \sin \frac{\theta}{2} \frac{(\mathbf{p} \times \boldsymbol{\sigma}_{s' s})_z}{|\mathbf{p}_\perp|}. \quad (8)$$

By comparing the expressions on the left-hand side of Eq. (7), obtained directly in the EF using Dirac bilinears [47], with the generic Lorentz transformation on the right-hand side from the transverse BF ( $P_z = 0$  and  $\Delta_z = 0$ ), we determine the Wigner rotation angle

$$\begin{aligned} \cos \theta &= \frac{P^0 + M(1 + \tau)}{(P^0 + M) \sqrt{1 + \tau}}, \\ \sin \theta &= -\frac{\sqrt{\tau} P_z}{(P^0 + M) \sqrt{1 + \tau}}, \end{aligned} \quad (9)$$

and the Lorentz boost parameters

$$d\gamma = \frac{P^0}{\sqrt{P^2}}, \quad \beta = \frac{P_z}{P^0}. \quad (10)$$

These coincide precisely with the results obtained in Ref. [23] in the case of the electromagnetic current. Note that both the Wigner rotation angle and the Lorentz boost parameters depend on the momentum transfer.

Since the total four-momentum operator is defined as  $\hat{P}^\mu = \int d^3 r \hat{T}^{0\mu}(\mathbf{r})$ , we find that

$$\int d^2 b_\perp T^{\mu\nu}(\mathbf{b}_\perp, P_z; s', s) = M \frac{u^\mu u^\nu}{u^0} \delta_{s' s} \quad (11)$$

with  $u^\mu = \gamma_P(1, \mathbf{0}_\perp, \beta_P)$  the four-velocity of the system. The Lorentz boost parameters are given by

$$\gamma_P = \frac{E_P}{M}, \quad \beta_P = \frac{P_z}{E_P} \quad (12)$$

with  $E_P = \sqrt{P_z^2 + M^2}$ , and coincide with the forward limit  $\Delta \rightarrow 0$  of the expressions in Eq. (10). It is clear from Eq. (11) that the spatial distributions  $T^{00}$ ,  $T^{03}$ ,  $T^{30}$ , and  $T^{33}$  diverge in the IMF. Since our goal is to discuss the distortions induced by a Lorentz boost along the  $z$ -direction, we factor out the trivial Lorentz factors and define EMT distributions with  $P_z$ -independent normalizations. Namely, we consider similarly to Ref. [17]

$$t_a^{\mu\nu} := \gamma_P T_a^{\mu\nu} = \begin{pmatrix} \gamma_P^2 \rho_a & \gamma_P \mathcal{P}_a^i & \gamma_P^2 \mathcal{P}_a^z \\ \gamma_P \mathcal{I}_a^i & \Pi_a^{ij} & \gamma_P \Pi_a^{iz} \\ \gamma_P^2 \mathcal{I}_a^z & \gamma_P \Pi_a^{zi} & \gamma_P^2 \Pi_a^{zz} \end{pmatrix}, \quad (13)$$

where the indices  $i, j = x, y$  denote transverse components.

In this paper, we focus on the ‘‘longitudinal’’ components  $T^{00}$ ,  $T^{03}$ ,  $T^{30}$ , and  $T^{33}$ . The other components of the EMT do not mix with these under a longitudinal Lorentz boost and will be discussed in a future work [48]. We find that the EF amplitudes are given by

$$\begin{aligned} \left. \frac{\langle p', s' | \hat{T}_a^{00}(0) | p, s \rangle}{2P^0} \right|_{\text{EF}} &= \gamma \left[ \cos \theta \delta_{s's} + \sin \theta \frac{(\boldsymbol{\sigma}_{s's} \times i\boldsymbol{\Delta}_\perp)_z}{2M\sqrt{\tau}} \right] M [E_a(Q^2) + \beta^2 F_a(Q^2)] \\ &+ \gamma \beta \left[ \cos \theta \frac{(\boldsymbol{\sigma}_{s's} \times i\boldsymbol{\Delta}_\perp)_z}{2M\sqrt{\tau}} - \sin \theta \delta_{s's} \right] 2M\sqrt{\tau} J_a(Q^2), \end{aligned} \quad (14a)$$

$$\begin{aligned} \left. \frac{\langle p', s' | \hat{T}_a^{03}(0) | p, s \rangle}{2P^0} \right|_{\text{EF}} &= \gamma \beta \left[ \cos \theta \delta_{s's} + \sin \theta \frac{(\boldsymbol{\sigma}_{s's} \times i\boldsymbol{\Delta}_\perp)_z}{2M\sqrt{\tau}} \right] M [E_a(Q^2) + F_a(Q^2)] \\ &+ \gamma \left[ \cos \theta \frac{(\boldsymbol{\sigma}_{s's} \times i\boldsymbol{\Delta}_\perp)_z}{2M\sqrt{\tau}} - \sin \theta \delta_{s's} \right] M\sqrt{\tau} [(1 + \beta^2) J_a(Q^2) - (1 - \beta^2) S_a(Q^2)], \end{aligned} \quad (14b)$$

$$\begin{aligned} \left. \frac{\langle p', s' | \hat{T}_a^{33}(0) | p, s \rangle}{2P^0} \right|_{\text{EF}} &= \gamma \left[ \cos \theta \delta_{s's} + \sin \theta \frac{(\boldsymbol{\sigma}_{s's} \times i\boldsymbol{\Delta}_\perp)_z}{2M\sqrt{\tau}} \right] M [\beta^2 E_a(Q^2) + F_a(Q^2)] \\ &+ \gamma \beta \left[ \cos \theta \frac{(\boldsymbol{\sigma}_{s's} \times i\boldsymbol{\Delta}_\perp)_z}{2M\sqrt{\tau}} - \sin \theta \delta_{s's} \right] 2M\sqrt{\tau} J_a(Q^2), \end{aligned} \quad (14c)$$

where we defined energy, TAM and force FFs as

$$\begin{aligned} E_a &= A_a - \tau B_a + \bar{C}_a + \tau D_a, \\ J_a &= \frac{A_a + B_a}{2}, \\ F_a &= -\bar{C}_a - \tau D_a. \end{aligned} \quad (15)$$

These are the natural combinations that appear in the

BF. The matrix elements of  $\hat{T}_a^{30}$  are obtained through the substitution  $S_a \mapsto -S_a$  in the matrix elements of  $\hat{T}_a^{03}$ . Since  $\beta \rightarrow 1$  when  $P_z \rightarrow \infty$ , all the amplitudes in Eq. (14) become equal in the IMF.

The normalized distributions of energy  $\rho_a$ , longitudinal momentum  $\mathcal{P}_a^z$ , longitudinal energy flux  $\mathcal{I}_a^z$ , and longitudinal thrust  $\Pi_a^{zz}$  can therefore be expressed as

$$g_a(\mathbf{b}_\perp, P_z; s', s) = \int \frac{d^2 \Delta_\perp}{(2\pi)^2} e^{-i\boldsymbol{\Delta}_\perp \cdot \mathbf{b}_\perp} \left[ \delta_{s's} \tilde{g}_a^U(Q^2, P_z) + \frac{(\boldsymbol{\sigma}_{s's} \times i\boldsymbol{\Delta}_\perp)_z}{2M} \tilde{g}_a^T(Q^2, P_z) \right] \quad (16)$$

with  $g = \rho, \mathcal{P}^z, \mathcal{I}^z, \Pi^{zz}$ . The superscripts  $U$  and  $T$  denote the unpolarized and transversely polarized contributions, respectively. Note that these EMT distributions are not affected by the nucleon longitudinal polarization.

The unpolarized EF distributions are defined as [17]

$$\begin{aligned} g_a(b, P_z) &:= \frac{1}{2} \sum_{s', s} g_a(\mathbf{b}_\perp, P_z; s', s) \delta_{s's} \\ &= \int \frac{d^2 \Delta_\perp}{(2\pi)^2} e^{-i\boldsymbol{\Delta}_\perp \cdot \mathbf{b}_\perp} \tilde{g}_a^U(Q^2, P_z) \end{aligned} \quad (17)$$

with  $b = |\mathbf{b}_\perp|$ . The axial symmetry is broken by the nucleon transverse polarization. In the following, we will consider the case of a nucleon polarized in the  $x$ -direction. Its spin state is then given by  $|s_x = \pm \frac{1}{2}\rangle =$

$(|s = +\frac{1}{2}\rangle \pm |s = -\frac{1}{2}\rangle) / \sqrt{2}$  and the corresponding EF distributions are defined as

$$\begin{aligned} g_a^P(\mathbf{b}_\perp, P_z) &:= g_a(\mathbf{b}_\perp, P_z; s'_x = +\frac{1}{2}, s_x = +\frac{1}{2}), \\ &= \int \frac{d^2 \Delta_\perp}{(2\pi)^2} e^{-i\boldsymbol{\Delta}_\perp \cdot \mathbf{b}_\perp} \\ &\times \left[ \tilde{g}_a^U(Q^2, P_z) + \frac{i\Delta_y}{2M} \tilde{g}_a^T(Q^2, P_z) \right]. \end{aligned} \quad (18)$$

## B. Energy distribution

The spin-independent and spin-dependent amplitudes defining the EF energy distribution are given by

$$\tilde{\rho}_a^U(Q^2, P_z) = \frac{1}{\gamma_P} \frac{P^0 [P^0 + M(1 + \tau)]}{(P^0 + M)(1 + \tau)} \left\{ E_a(Q^2) + \frac{2\tau P_z^2}{P^0 [P^0 + M(1 + \tau)]} J_a(Q^2) + \left( \frac{P_z}{P^0} \right)^2 F_a(Q^2) \right\}, \quad (19a)$$

$$\tilde{\rho}_a^T(Q^2, P_z) = \frac{1}{\gamma_P} \frac{P^0 P_z}{(P^0 + M)(1 + \tau)} \left\{ -E_a(Q^2) + \frac{2[P^0 + M(1 + \tau)]}{P^0} J_a(Q^2) - \left( \frac{P_z}{P^0} \right)^2 F_a(Q^2) \right\}, \quad (19b)$$

and the total EF energy distribution is normalized as

$$\int d^2b_\perp \rho(\mathbf{b}_\perp, P_z; s', s) = \tilde{g}^U(0, P_z) \delta_{s's} = M \delta_{s's} \quad (20)$$

since  $E(0) = 1$  and  $F(0) = 0$ .

In the transverse BF, the energy amplitudes reduce to

$$\begin{aligned} \tilde{\rho}_a^U(Q^2, 0) &= M E_a(Q^2), \\ \tilde{\rho}_a^T(Q^2, 0) &= 0, \end{aligned} \quad (21)$$

in agreement with the results in Refs. [3, 17]. All the terms associated with explicit factors of  $P_z$  in Eq. (19) can then be understood as contributions induced by the Lorentz boost from the BF to the EF. In the IMF, we find that

$$\begin{aligned} \tilde{\rho}_a^U(Q^2, \infty) &= M A_a(Q^2), \\ \tilde{\rho}_a^T(Q^2, \infty) &= M B_a(Q^2). \end{aligned} \quad (22)$$

In Fig. 1, we show the quark and gluon contributions to the EF energy distribution in an unpolarized nucleon at various values of  $P_z$ . Since these distributions are axially symmetric, only the radial profile is displayed. As  $P_z$  increases, the contribution associated with  $E_a$  decreases near the center while the induced contributions associated with  $J_a$  and  $F_a$  increase. We observe that the contribution associated with  $F_q$  is much larger than that associated with  $F_G$ . This difference finds its origin in the fact that  $\tilde{C}_q(Q^2) = -\tilde{C}_G(Q^2)$ .

In Fig. 2, we illustrate the same distributions for the nucleon polarized along the  $x$ -direction. Since the axial symmetry is broken in this case, we show the profile at  $b_x = 0$ . We find that the dipole shift induced by the contribution associated with  $J_a$  goes in the opposite direction to those associated with  $E_a$  and  $F_a$ . In the absence

of Wigner rotation, only the former would play a role. As shown in Fig. 3, a dipolar distortion along the  $y$ -axis appears in the total EF energy distribution for non-zero  $P_z$ . The fact that this dipolar distortion disappears in the IMF is an artifact of the naive multipole model of Ref. [17], which assumed  $B_q(Q^2) = -B_G(Q^2)$  due to the lack of information on the gluon GFFs. In a more realistic description, we expect a priori  $B_q(Q^2) \neq -B_G(Q^2)$  and hence a dipolar distortion in the IMF similar to what is observed for the charge distribution [23, 39].

The total EF energy dipole moment

$$\begin{aligned} \int d^2b_\perp \mathbf{b}_\perp \rho(\mathbf{b}_\perp, P_z; s', s) &= \frac{(\mathbf{e}_z \times \boldsymbol{\sigma}_{s's})_z}{2M} \tilde{\rho}^T(0, P_z) \\ &= (\mathbf{e}_z \times \boldsymbol{\sigma}_{s's})_z \frac{P_z}{E_P} \left[ J(0) - \frac{E_P}{E_P + M} \frac{E(0)}{2} \right] \end{aligned} \quad (23)$$

has the same structure as the EF electric dipole moment [41]. The first contribution corresponds to the longitudinal boost of a rest-frame transverse TAM and has the expected form  $\boldsymbol{\beta}_P \times \mathbf{J}$ . The second contribution comes from a sideways shift of the center of spin, defining the origin of our coordinate system, with respect to the relativistic center of mass in a moving frame [38, 49]. In the IMF, this dipole moment vanishes as a consequence of  $B(0) = 0$ .

### C. Longitudinal momentum and longitudinal energy flux distributions

The spin-independent and spin-dependent amplitudes defining the longitudinal momentum distribution in the EF are given by

$$\begin{aligned} \tilde{\mathcal{P}}_a^{z,U}(Q^2, P_z) &= \frac{1}{\gamma_P} \frac{P_z [P^0 + M(1 + \tau)]}{(P^0 + M)(1 + \tau)} \\ &\times \left\{ E_a(Q^2) + \frac{\tau P^2}{P^0 [P^0 + M(1 + \tau)]} \left[ \left( \frac{2P_z^2}{P^2} + 1 \right) J_a(Q^2) - S_a(Q^2) \right] + F_a(Q^2) \right\}, \end{aligned} \quad (24a)$$

## EF energy distributions for an unpolarized nucleon

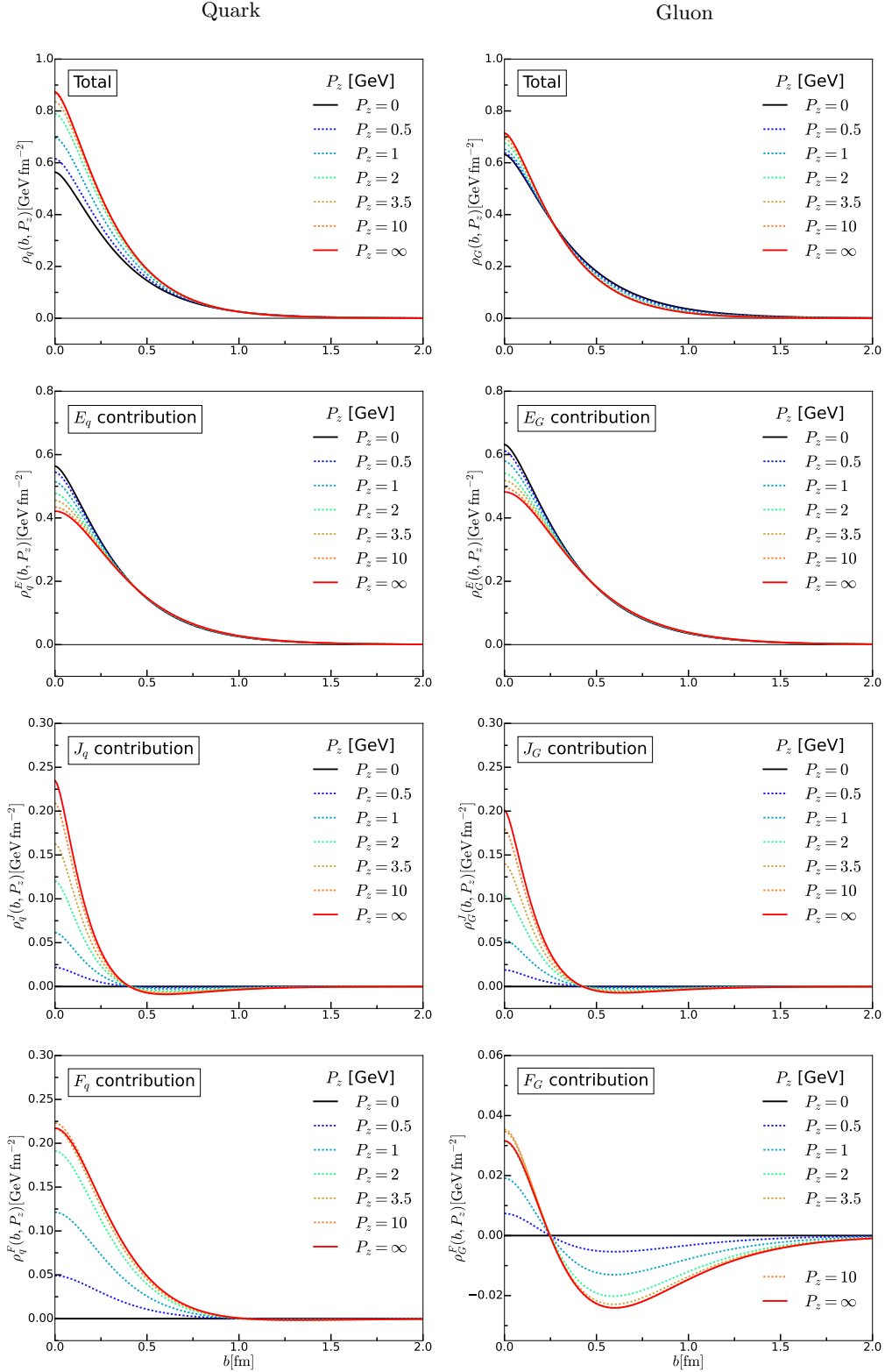


FIG. 1: Radial EF energy distributions in an unpolarized nucleon for different values of the nucleon momentum. The total energy distribution is normalized to  $M$ . The left (right) column corresponds to the quark (gluon) contribution. The first row depicts the sum of the three contributions shown in the other rows. Based on the simple multipole model of Ref. [17] for the EMT FFs.

### EF energy distributions for a transversely polarized nucleon

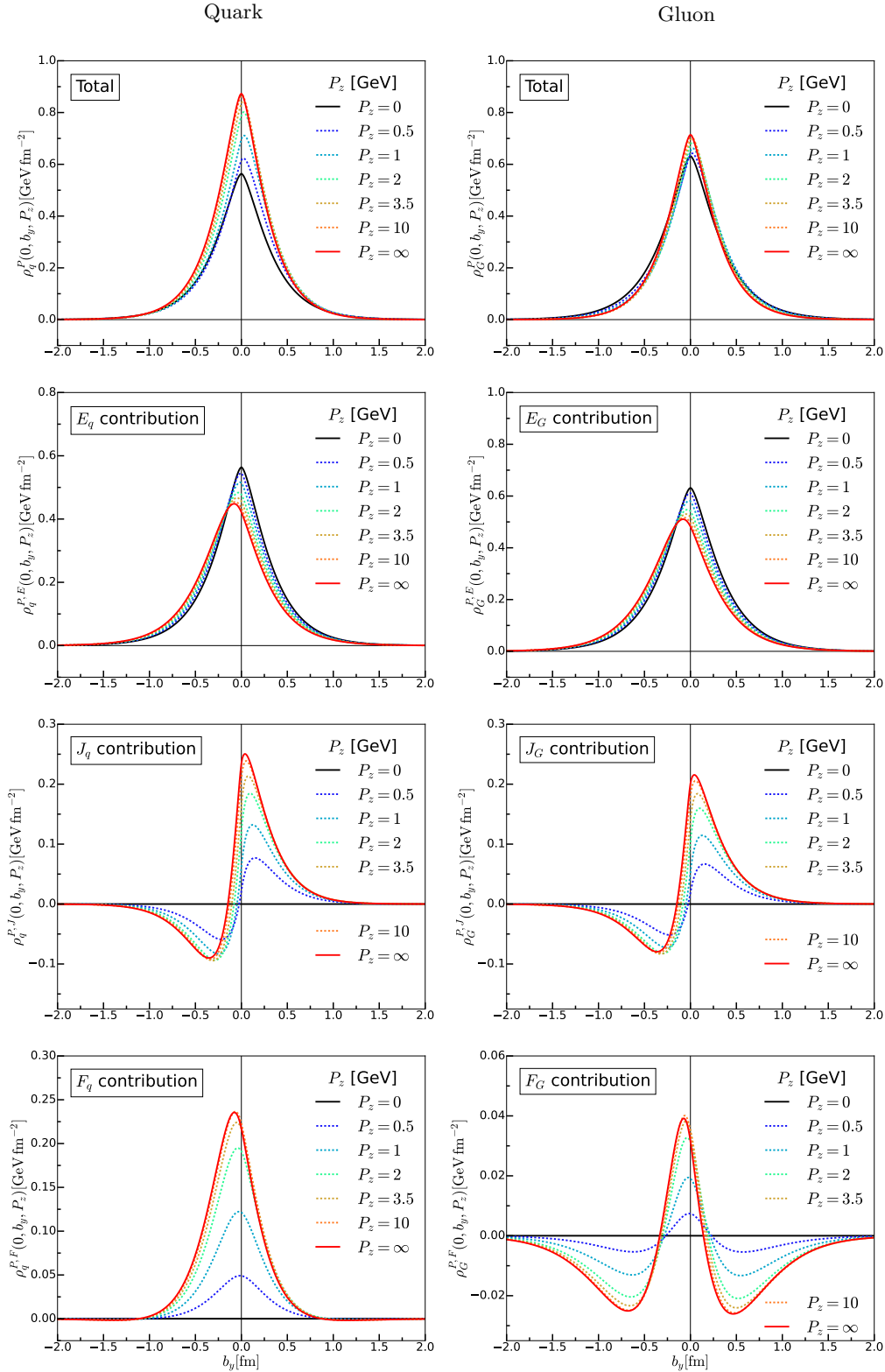


FIG. 2: EF energy distributions at  $b_x = 0$  in a nucleon polarized along the  $x$ -axis for different values of the nucleon momentum. The total energy distribution is normalized to  $M$ . The left (right) column corresponds to the quark (gluon) contribution. The first row depicts the sum of the three contributions shown in the other rows. Based on the simple multipole model of Ref. [17] for the EMT FFs.

**Total EF energy distribution for a transversely polarized nucleon**

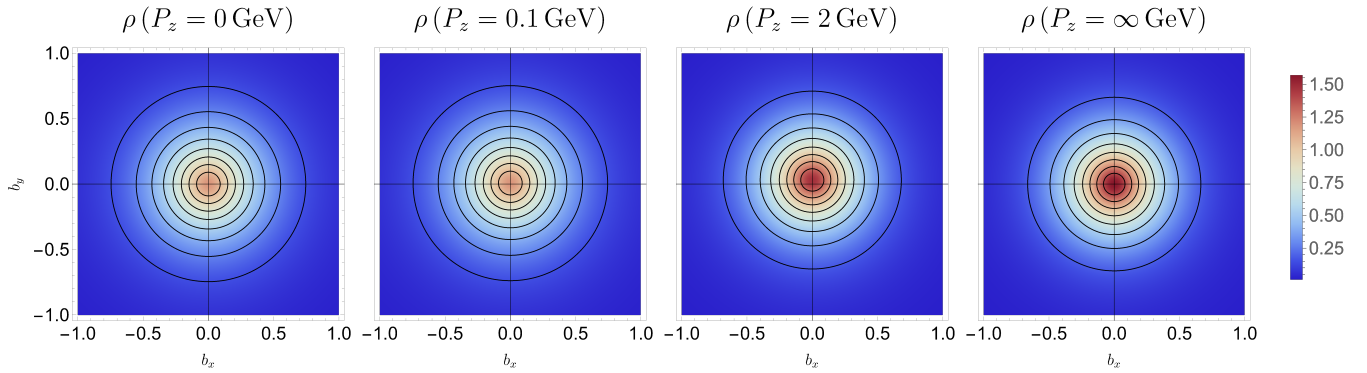


FIG. 3: Total EF energy distributions in the transverse plane of a nucleon polarized along the  $x$ -axis for different values of the nucleon momentum. The total energy distribution is normalized to  $M$ . Based on the simple multipole model of Ref. [17] for the EMT FFs.

$$\begin{aligned} \tilde{\mathcal{P}}_a^{z,T}(Q^2, P_z) &= \frac{1}{\gamma_P} \frac{P^2}{(P^0 + M)(1 + \tau)} \\ &\times \left\{ -\frac{P_z^2}{P^2} E_a(Q^2) + \frac{P^0 + M(1 + \tau)}{P^0} \left[ \left( \frac{2P_z^2}{P^2} + 1 \right) J_a(Q^2) - S_a(Q^2) \right] - \frac{P_z^2}{P^2} F_a(Q^2) \right\}. \end{aligned} \quad (24b)$$

For the longitudinal energy flux distribution in the EF, the spin-independent and spin-dependent amplitudes  $\tilde{\mathcal{I}}_a^{z,U}$  and  $\tilde{\mathcal{I}}_a^{z,T}$  are obtained by reversing the sign of the spin FF. The total EF distribution of longitudinal momentum is normalized as

$$\int d^2 b_\perp \mathcal{P}^z(\mathbf{b}_\perp, P_z; s', s) = M\beta_P \delta_{s's}, \quad (25)$$

and similarly for the total EF distribution of longitudinal energy flux  $\mathcal{I}^z$ .

In the transverse BF, the longitudinal momentum and longitudinal energy flux amplitudes reduce to

$$\begin{aligned} \tilde{\mathcal{P}}_a^{z,U}(Q^2, 0) &= \tilde{\mathcal{I}}_a^{z,U}(Q^2, 0) = 0, \\ \tilde{\mathcal{P}}_a^{z,T}(Q^2, 0) &= M [J_a(Q^2) - S_a(Q^2)], \\ \tilde{\mathcal{I}}_a^{z,T}(Q^2, 0) &= M [J_a(Q^2) + S_a(Q^2)], \end{aligned} \quad (26)$$

in agreement with the results in Refs. [3, 17]. All the terms associated with explicit factors of  $P_z$  in Eq. (24) can then be understood as contributions induced by the Lorentz boost from the BF to the EF. In the IMF, we find that

$$\begin{aligned} \tilde{\mathcal{P}}_a^{z,U}(Q^2, \infty) &= \tilde{\mathcal{I}}_a^{z,U}(Q^2, \infty) = M A_a(Q^2), \\ \tilde{\mathcal{P}}_a^{z,T}(Q^2, \infty) &= \tilde{\mathcal{I}}_a^{z,T}(Q^2, \infty) = M B_a(Q^2). \end{aligned} \quad (27)$$

In Fig. 4, we compare the total EF distributions of longitudinal momentum and longitudinal energy flux in the

transverse plane for non-zero  $P_z$ . The differences result directly from the fact that the contribution associated with  $S_a$  enters with an opposite sign in these two distributions. In the IMF, however,  $\mathcal{P}^z$  and  $\mathcal{I}^z$  become equal because the spin contribution is kinematically suppressed at large  $P_z$ .

Contrary to the energy dipole moment, the dipole moment of the longitudinal momentum distribution does not vanish in the BF, but is given by

$$\int d^2 b_\perp \mathbf{b}_\perp \mathcal{P}^z(\mathbf{b}_\perp, 0; s', s) = (\mathbf{e}_z \times \boldsymbol{\sigma}_{s's})_z \frac{1}{2} L(0), \quad (28)$$

where  $L(Q^2) = J(Q^2) - S(Q^2)$  is the OAM FF. Since the 3D BF momentum distributions

$$\begin{aligned} \mathcal{P}^\mu(\mathbf{r}; s', s) &= \langle \hat{T}^{0\mu}(\mathbf{r}) \rangle_{\mathbf{0}, \mathbf{0}; s', s} \\ &= \int \frac{d^3 \Delta}{(2\pi)^3} e^{-i\boldsymbol{\Delta} \cdot \mathbf{r}} \frac{\langle p', s' | \hat{T}^{0\mu}(0) | p, s \rangle}{2P^0} \Big|_{\text{BF}} \end{aligned} \quad (29)$$

are axially symmetric about the polarization axis, we indeed expect for a nucleon polarized along the  $x$ -direction that

$$\int d^3 r y \mathcal{P}^z(\mathbf{r}) = \frac{1}{2} \int d^3 r [y \mathcal{P}^z(\mathbf{r}) - z \mathcal{P}^y(\mathbf{r})]. \quad (30)$$

In other words, the dipole moment in the BF momentum distribution is a direct manifestation of the internal OAM.

**Total EF distributions of longitudinal momentum and longitudinal energy flux for a transversely polarized nucleon**

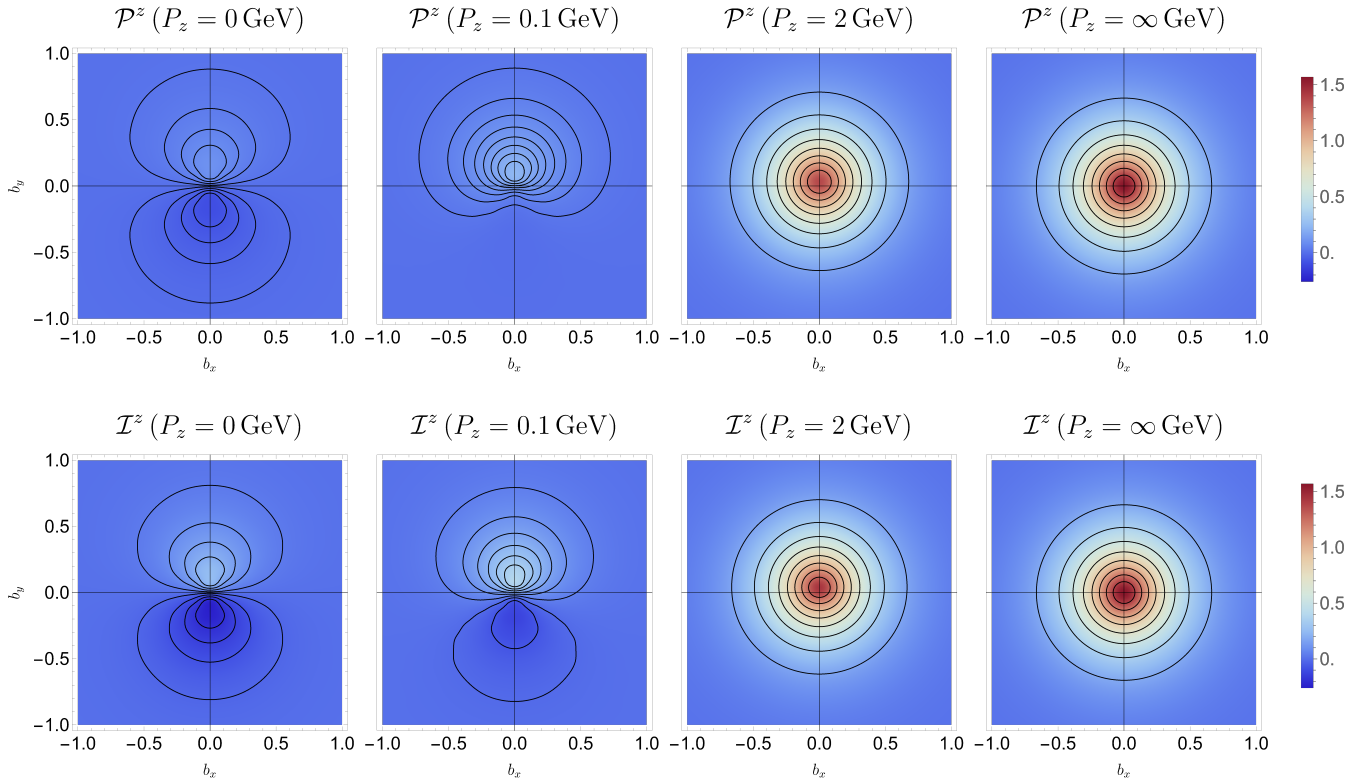


FIG. 4: Total EF frame distributions of longitudinal momentum and longitudinal energy flux in the transverse plane of a nucleon polarized along the  $x$ -axis for different values of the nucleon momentum. The total distributions are normalized to  $M\beta_P$ . Based on the simple multipole model of Ref. [17] for the EMT FFs.

Similarly, the dipole moment of the longitudinal energy flux distribution is given in the BF by

$$\int d^2b_\perp \mathbf{b}_\perp \mathcal{I}^z(\mathbf{b}_\perp, 0; s', s) = (\mathbf{e}_z \times \boldsymbol{\sigma}_{s's})_z \frac{1}{2} [L(0) + 2S(0)], \quad (31)$$

In particular, even in the absence of internal OAM, there

is still a circulation of energy due to the intrinsic spin.

#### D. Longitudinal thrust distribution

The spin-independent and spin-dependent amplitudes defining the longitudinal thrust distribution in the EF are given by

$$\tilde{\Pi}_a^{zz,U}(Q^2, P_z) = \frac{1}{\gamma_P} \frac{P^0 [P^0 + M(1 + \tau)]}{(P^0 + M)(1 + \tau)} \left\{ \left( \frac{P_z}{P^0} \right)^2 E_a(Q^2) + \frac{2\tau P_z^2}{P^0 [P^0 + M(1 + \tau)]} J_a(Q^2) + F_a(Q^2) \right\}, \quad (32a)$$

$$\tilde{\Pi}_a^{zz,T}(Q^2, P_z) = \frac{1}{\gamma_P} \frac{P^0 P_z}{(P^0 + M)(1 + \tau)} \left\{ - \left( \frac{P_z}{P^0} \right)^2 E_a(Q^2) + \frac{2 [P^0 + M(1 + \tau)]}{P^0} J_a(Q^2) - F_a(Q^2) \right\}, \quad (32b)$$

and the total EF distribution of longitudinal thrust is normalized as

$$\int d^2b_\perp \Pi^{zz}(\mathbf{b}_\perp, P_z; s', s) = M\beta_P^2 \delta_{s's}. \quad (33)$$

In the transverse BF, the longitudinal thrust amplitudes reduce to

$$\begin{aligned} \tilde{\Pi}_a^{zz,U}(Q^2, 0) &= M F_a(Q^2), \\ \tilde{\Pi}_a^{zz,T}(Q^2, 0) &= 0. \end{aligned} \quad (34)$$

**Total EF distribution of longitudinal thrust for a transversely polarized nucleon**

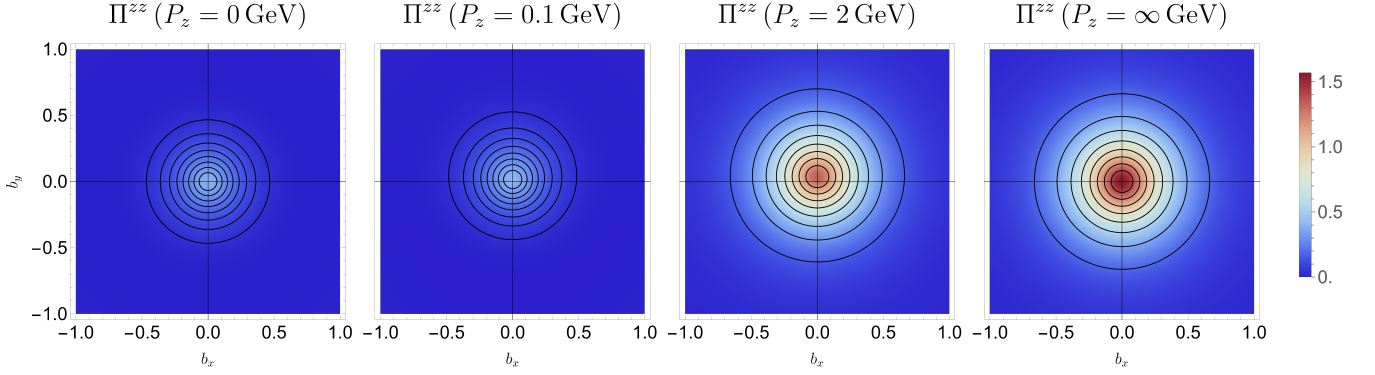


FIG. 5: Total EF frame distributions of longitudinal thrust in the transverse plane of a nucleon polarized along the  $x$ -axis for different values of the nucleon momentum. The total distributions are normalized to  $M\beta_P^2$ . Based on the simple multipole model of Ref. [17] for the EMT FFs.

in agreement with the results in Refs. [3, 17]. All the terms associated with explicit factors of  $P_z$  in Eq. (32) can then be understood as contributions induced by the Lorentz boost from the BF to the EF. In the IMF, we find that

$$\begin{aligned}\tilde{\Pi}_a^{zz,U}(Q^2, \infty) &= MA_a(Q^2), \\ \tilde{\Pi}_a^{zz,T}(Q^2, \infty) &= MB_a(Q^2),\end{aligned}\quad (35)$$

just like in the cases of the EF energy, longitudinal momentum, and longitudinal energy flux distributions, see Eqs. (22) and (27).

In Fig. 5, we show the total EF distributions of longitudinal thrust for non-zero  $P_z$ . The differences with the total EF energy distributions displayed in Fig. 3 are simply due to the different kinematical weighting of the contributions associated with  $E_a$  and  $F_a$ , see Eqs. (19) and (32). This explains also why the dipole moment of the total longitudinal thrust distribution in the EF

$$\begin{aligned}\int d^2b_\perp \mathbf{b}_\perp \Pi^{zz}(\mathbf{b}_\perp, P_z; s', s) &= (\mathbf{e}_z \times \boldsymbol{\sigma}_{s's})_z \\ &\times \frac{P_z}{E_P} \left[ J(0) - \frac{E_P}{E_P + M} \left( \frac{P_z}{E_P} \right)^2 \frac{E(0)}{2} \right]\end{aligned}\quad (36)$$

differs from the total EF energy dipole moment, except in the limit  $P_z \rightarrow \infty$ .

#### IV. DISTRIBUTIONS ON THE LIGHT FRONT

A key feature of the light-front (LF) formalism [50, 51] is that it exhibits Galilean symmetry in the transverse

plane. As a result, spatial densities with probabilistic interpretation and free of relativistic recoil corrections can, in some cases, be defined within this framework [13, 14]. This applies, in particular, to the EMT component  $T^{++}$  [14, 20], which is interpreted as the LF density of longitudinal momentum.

By adapting the phase-space formalism to the LF picture, one can define 2D LF distributions for all the EMT components as follows [17]

$$\begin{aligned}T_a^{\mu\nu}(\mathbf{b}_\perp, P^+; \lambda', \lambda) &= \int \frac{d^2\Delta_\perp}{(2\pi)^2} e^{-i\Delta_\perp \cdot \mathbf{b}_\perp} \\ &\times \frac{\text{LF}\langle p', \lambda' | \hat{T}_a^{\mu\nu}(0) | p, \lambda \rangle_{\text{LF}}}{2P^+} \Bigg|_{\text{DYF}},\end{aligned}\quad (37)$$

where  $|p, \lambda\rangle_{\text{LF}}$  is a LF four-momentum eigenstate with LF helicity  $\lambda$ . LF components are defined as  $x^\mu = [x^+, x^-, \mathbf{x}_\perp]$  with  $x^\pm = (x^0 \pm x^3)/\sqrt{2}$ . The symmetric Drell-Yan frame (DYF), characterized by  $\Delta^+ = 0$  and  $\mathbf{P}_\perp = \mathbf{0}_\perp$ , ensures that the LF energy transfer vanishes  $\Delta^- = (\Delta_\perp \cdot \mathbf{P}_\perp - \Delta^+ P^-)/P^+ = 0$ . It follows that the 2D LF distributions remain  $x^+$ -independent [26].

Focusing of the “longitudinal” LF components  $T^{++}$ ,  $T^{+-}$ ,  $T^{-+}$ , and  $T^{--}$ , we find that the LF amplitudes are given by

$$\langle p', \lambda' | \hat{T}_a^{++}(0) | p, \lambda \rangle_{\text{LF}} \Big|_{\text{DYF}} = 2 (P^+)^2 \left\{ \delta_{\lambda' \lambda} A_a(Q^2) + \frac{(\boldsymbol{\sigma}_{\lambda' \lambda} \times i \boldsymbol{\Delta}_\perp)_z}{2M} B_a(Q^2) \right\}, \quad (38a)$$

$$\langle p', \lambda' | \hat{T}_a^{+-}(0) | p, \lambda \rangle_{\text{LF}} \Big|_{\text{DYF}} = \frac{2P^+ P^-}{1 + \tau} \left\{ \delta_{\lambda' \lambda} [E_a(Q^2) - F_a(Q^2) + 2\tau S_a(Q^2)] \right. \\ \left. - \frac{(\boldsymbol{\sigma}_{\lambda' \lambda} \times i \boldsymbol{\Delta}_\perp)_z}{2M} [E_a(Q^2) - F_a(Q^2) - 2S_a(Q^2)] \right\}, \quad (38b)$$

$$\langle p', \lambda' | \hat{T}_a^{--}(0) | p, \lambda \rangle_{\text{LF}} \Big|_{\text{DYF}} = \frac{2(P^-)^2}{1 + \tau} \left\{ \delta_{\lambda' \lambda} [(1 - \tau)A_a(Q^2) - 2\tau B_a(Q^2)] \right. \\ \left. - \frac{(\boldsymbol{\sigma}_{\lambda' \lambda} \times i \boldsymbol{\Delta}_\perp)_z}{2M} [2A_a(Q^2) + (1 - \tau)B_a(Q^2)] \right\}. \quad (38c)$$

The matrix element of  $\hat{T}_a^{+-}$  is obtained by reversing the sign of  $S_a$  in Eq. (38b). Note that we can write  $P^- = M^2(1 + \tau)/(2P^+)$ .

Similarly to the analysis presented in Ref. [23] for the

electromagnetic current, we can relate these LF amplitudes to the corresponding IMF amplitudes. Indeed, combining the results in Eq. (14), we find that

$$\langle p', s' | \hat{T}_a^{++}(0) | p, s \rangle_{\text{EF}} = \frac{2(P^+)^2}{\sqrt{1 + \tau}} \left\{ \delta_{s' s} [\cos \theta (E_a(Q^2) + F_a(Q^2)) - 2\sqrt{\tau} \sin \theta J_a(Q^2)] \right. \\ \left. + \frac{(\boldsymbol{\sigma}_{s' s} \times i \boldsymbol{\Delta}_\perp)_z}{2M\sqrt{\tau}} [\sin \theta (E_a(Q^2) + F_a(Q^2)) + 2\sqrt{\tau} \cos \theta J_a(Q^2)] \right\}, \quad (39a)$$

$$\langle p', s' | \hat{T}_a^{+-}(0) | p, s \rangle_{\text{EF}} = \frac{2P^+ P^-}{\sqrt{1 + \tau}} \left\{ \delta_{s' s} [\cos \theta (E_a(Q^2) - F_a(Q^2)) - 2\sqrt{\tau} \sin \theta S_a(Q^2)] \right. \\ \left. + \frac{(\boldsymbol{\sigma}_{s' s} \times i \boldsymbol{\Delta}_\perp)_z}{2M\sqrt{\tau}} [\sin \theta (E_a(Q^2) - F_a(Q^2)) + 2\sqrt{\tau} \cos \theta S_a(Q^2)] \right\}, \quad (39b)$$

$$\langle p', s' | \hat{T}_a^{--}(0) | p, s \rangle_{\text{EF}} = \frac{2(P^-)^2}{\sqrt{1 + \tau}} \left\{ \delta_{s' s} [\cos \theta (E_a(Q^2) + F_a(Q^2)) + 2\sqrt{\tau} \sin \theta J_a(Q^2)] \right. \\ \left. + \frac{(\boldsymbol{\sigma}_{s' s} \times i \boldsymbol{\Delta}_\perp)_z}{2M\sqrt{\tau}} [\sin \theta (E_a(Q^2) + F_a(Q^2)) - 2\sqrt{\tau} \cos \theta J_a(Q^2)] \right\}. \quad (39c)$$

In general, canonical polarization  $s$  differs from LF helicity  $\lambda$ . However, the difference disappears in the IMF,

where the Wigner rotation (9) reduces to

$$\lim_{P_z \rightarrow \infty} \cos \theta = \frac{1}{\sqrt{1 + \tau}}, \quad \lim_{P_z \rightarrow \infty} \sin \theta = -\frac{\sqrt{\tau}}{\sqrt{1 + \tau}}. \quad (40)$$

The spin-independent and spin-dependent contributions

to the IMF matrix element of  $\hat{T}^{++}$  are then driven by the following linear combinations of EMT FFs

$$\lim_{P_z \rightarrow \infty} \frac{\cos \theta (E_a + F_a) - 2\sqrt{\tau} \sin \theta J_a}{\sqrt{1 + \tau}} = A_a, \quad (41a)$$

$$\lim_{P_z \rightarrow \infty} \frac{\sin \theta (E_a + F_a) + 2\sqrt{\tau} \cos \theta J_a}{\sqrt{\tau} \sqrt{1 + \tau}} = B_a, \quad (41b)$$

in agreement with the LF amplitude (38a). Similarly, we find for the unpolarized and polarized contributions to the IMF matrix element of  $\hat{T}^{+-}$

$$\begin{aligned} \lim_{P_z \rightarrow \infty} \frac{\cos \theta (E_a - F_a) - 2\sqrt{\tau} \sin \theta S_a}{\sqrt{1 + \tau}} \\ = \frac{E_a - F_a + 2\tau S_a}{1 + \tau}, \end{aligned} \quad (42a)$$

$$\begin{aligned} \lim_{P_z \rightarrow \infty} \frac{\sin \theta (E_a - F_a) + 2\sqrt{\tau} \cos \theta S_a}{\sqrt{\tau} \sqrt{1 + \tau}} \\ = \frac{-E_a + F_a + 2S_a}{1 + \tau}, \end{aligned} \quad (42b)$$

and of  $\hat{T}^{--}$

$$\begin{aligned} \lim_{P_z \rightarrow \infty} \frac{\cos \theta (E_a + F_a) + 2\sqrt{\tau} \sin \theta J_a}{\sqrt{1 + \tau}} \\ = \frac{(1 - \tau) A_a - 2\tau B_a}{1 + \tau}, \end{aligned} \quad (43a)$$

$$\begin{aligned} \lim_{P_z \rightarrow \infty} \frac{\sin \theta (E_a + F_a) - 2\sqrt{\tau} \cos \theta J_a}{\sqrt{\tau} \sqrt{1 + \tau}} \\ = \frac{-2A_a - (1 - \tau) B_a}{1 + \tau}, \end{aligned} \quad (43b)$$

which also agree with the LF expressions in Eqs. (38b) and (38c).

## V. SUMMARY

In this paper, we have studied the relativistic distributions of the local gauge-invariant and asymmetric energy-momentum tensor (EMT) current within the framework of the quantum phase-space formalism for the nucleons, taking into account for the first time the nucleon transverse polarization. We have focused on the ‘‘longitudinal’’ components of the EMT and defined the corresponding scaled distributions of energy, longitudinal momentum, longitudinal energy flux, and longitudinal thrust, including their decomposition into quark and gluon contributions. The frame dependence of these distributions has then been studied in detail and illustrated using a simple multipole model for the EMT form factors.

More specifically, we have demonstrated that the spin structure of the EMT matrix elements is the simplest in

the Breit frame, which can be thought of as the average rest frame of the system. The latter is therefore the natural frame for defining the intrinsic EMT distributions. We have also explicitly shown that the structure of the relativistic distributions for arbitrary values of the nucleon longitudinal momentum results from a combination of both the familiar mixing of the rank-two tensor components under a longitudinal boost and the Wigner spin rotation. In the infinite-momentum frame, all the ‘‘longitudinal’’ distributions become equal. The mixing of components under a longitudinal boost can be avoided by switching to the light-front components. In this form, we have shown that not only the ‘‘good’’  $T^{++}$  but also the ‘‘bad’’  $T^{+-}, T^{-+}, T^{--}$  distributions coincide in the infinite-momentum frame with those defined within the light-front formalism.

## VI. ACKNOWLEDGMENTS

This work is supported by the France Excellence scholarship through Campus France funded by the French government (Ministère de l’Europe et des Affaires Étrangères), Grant No. 141295X (H.-Y.W.).

### Appendix A: Quark axial singlet dipole mass

In this Appendix, we discuss in more detail the parametrization of the quark spin FF used to illustrate the EMT distributions in the EF. Many studies have been devoted to the axial iso-vector FF, based either on experiments involving neutrino-nucleus scattering [52–58] or on a variety of theoretical frameworks [59–70], see also the review [71]. In contrast, the axial flavor-singlet FF is less well known.

In order to determine an appropriate value for the axial singlet dipole mass, we focus on the BF longitudinal momentum distribution in the transverse plane for a nucleon polarized along the  $x$ -axis

$$\mathcal{P}_a^{z,P}(\mathbf{b}_\perp, 0) = M \int \frac{d^2 \Delta_\perp}{(2\pi)^2} e^{-i\Delta_\perp \cdot \mathbf{b}_\perp} \frac{i\Delta_y}{2M} L_a(Q^2), \quad (A1)$$

where the OAM FF is defined by  $L_a = J_a - S_a$ . Since the gluon spin FF is zero, we consider only the quark part.

In Fig. 6, we show how the quark OAM FF changes as the axial singlet dipole mass  $\Lambda_{S_q}$  varies. The value of  $Q^2$  at which the quark OAM FF becomes negative decreases with increasing values of  $\Lambda_{S_q}$ . This sign change leads to a node in the BF longitudinal momentum distribution along the radial direction in the transverse plane, depicted in Fig. 7. While the value of the total quark OAM  $L_q(0)$  does not depend on the axial singlet dipole mass, its spatial distribution does. For  $\Lambda_{S_q} = 1.00$  GeV, the polarity of the dipole pattern agrees with our expectation of a positive quark OAM along the  $x$ -axis. For

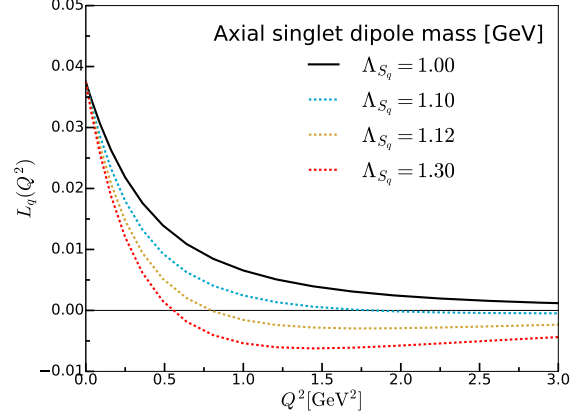


FIG. 6: Dependence of the quark OAM FF on the quark axial singlet dipole mass  $\Lambda_{S_q}$ .

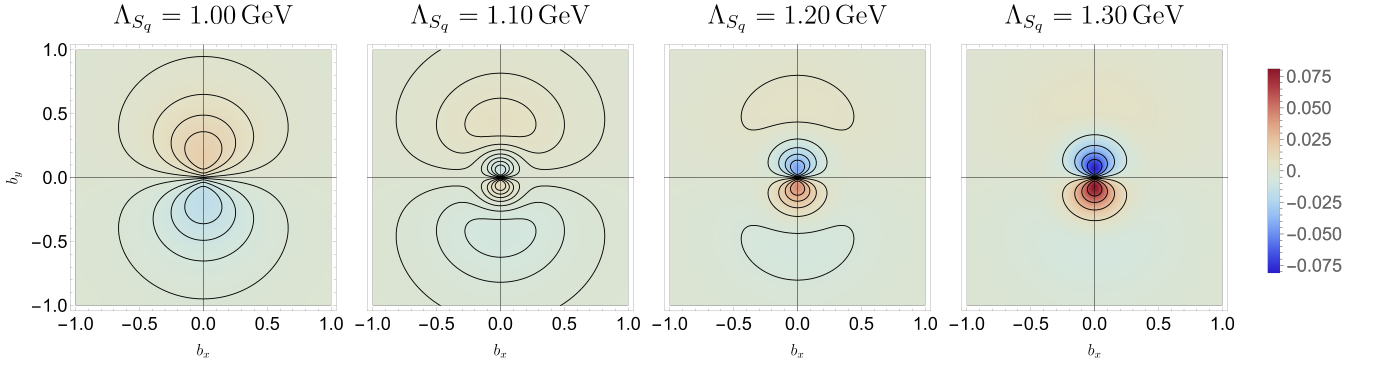


FIG. 7: Evolution of the BF distribution of longitudinal momentum in the transverse plane for different values of the quark axial singlet dipole mass  $\Lambda_{S_q}$ .

larger values of the dipole mass, the dipole pattern with the expected polarity spreads out in the transverse plane, diminishes in magnitude, and is gradually overshadowed by a new dipole pattern with opposite polarity. For the sake of simplicity, in this work we have adopted the value  $\Lambda_{S_q} = 1.00$  GeV to ensure that  $L_q(Q^2) > 0$  and thus avoid the appearance of a dipole pattern with the unexpected polarity. Note, however, that the polarity flip is in principle allowed and has been observed in the spatial distribution of  $d$ -quark average transverse momentum inside a longitudinally polarized nucleon, calculated within

some light-front quark models [72].

## Appendix B: Breit frame multipole form factors

Since the physics is more transparent when expressed in terms of the BF amplitudes, we find as with the electromagnetic current [21] that the EMT matrix elements can alternatively be parametrized in terms of the BF multipole FFs

$$\langle p', s' | \hat{T}_a^{\mu\nu}(0) | p, s \rangle = \bar{u}(p', s') \left[ M \frac{P^\mu P^\nu}{P^2} E_a(Q^2) + \frac{\Delta^\mu \Delta^\nu - \frac{1}{3} g_P^{\mu\nu} \Delta^2}{4M} F_{2,a}(Q^2) - M g_P^{\mu\nu} F_{0,a}(Q^2) \right. \\ \left. + \frac{i P^{\{\mu} \epsilon^{\nu\} \alpha\beta\rho} \Delta_\alpha P_\beta \gamma_\rho \gamma_5}{2P^2} J_a(Q^2) - \frac{i}{2} \epsilon^{\mu\nu\alpha\beta} \Delta_\alpha \gamma_\beta \gamma_5 S_a(Q^2) \right] u(p, s), \quad (\text{B1})$$

where  $g_P^{\mu\nu} = g^{\mu\nu} - P^\mu P^\nu / P^2$  is the projector onto the subspace orthogonal to  $P$ . The force FF driving the longitudinal thrust in the transverse BF (34) is given by a linear combination of a monopole and a quadrupole FF, viz.  $F_a = F_{0,a} - \frac{\tau}{3} F_{2,a}$  with  $F_{0,a} = -\bar{C}_a - \frac{2}{3}\tau D_a$  and  $F_{2,a} = D_a$ .

### Appendix C: Spatial distributions of longitudinal momentum and longitudinal thrust

In Figs. 8 and 9, we show the quark and gluon contributions to the EF distributions of, respectively, longitudinal momentum and longitudinal thrust in an unpolarized nucleon at various values of  $P_z$ . Since these distributions are axially symmetric, only the radial profiles are displayed.

Note that the longitudinal momentum distributions are purely induced by the Lorentz boost. In the absence of Wigner rotation, only the contributions associated with  $E_a$  and  $F_a$  would play a role. At large  $P_z$ , the contribution associated with  $S_a$  is the only one that is suppressed kinematically. The longitudinal thrust distributions are similar to the energy distributions. The difference in the  $P_z$ -evolution between the contributions associated with  $E_a$  and  $F_a$  is essentially a reflection of the relative kinematical weight  $\beta^2$  in Eqs. (14a) and (14c).

In Fig. 10 and 11, we illustrate the same distributions for the nucleon polarized along the  $x$ -direction. Similarly to the polarized EF energy distributions, the dipole shift induced by the contribution associated with  $J_a$  goes in the opposite direction to those associated with  $E_a$  and  $F_a$ .

- 
- [1] A. Accardi et al., Eur. Phys. J. A **52**, 268 (2016), 1212.1701.
- [2] R. Abdul Khalek et al., Nucl. Phys. A **1026**, 122447 (2022), 2103.05419.
- [3] M. V. Polyakov and P. Schweitzer, Int. J. Mod. Phys. A **33**, 1830025 (2018), 1805.06596.
- [4] V. D. Burkert, L. Elouadrhiri, F. X. Girod, C. Lorcé, P. Schweitzer, and P. E. Shanahan, Rev. Mod. Phys. **95**, 041002 (2023), 2303.08347.
- [5] X.-D. Ji, Phys. Rev. Lett. **78**, 610 (1997), hep-ph/9603249.
- [6] M. Diehl, Phys. Rept. **388**, 41 (2003), hep-ph/0307382.
- [7] C. Lorcé, Phys. Lett. B **735**, 344 (2014), 1401.7784.
- [8] J.-Y. Kim, H.-Y. Won, H.-C. Kim, and C. Weiss, Phys. Rev. D **110**, 054026 (2024), 2403.07186.
- [9] S. Bhattacharya, R. Boussarie, and Y. Hatta, Phys. Lett. B **859**, 139134 (2024), 2404.04208.
- [10] C. Lorcé and Q.-T. Song (2025), 2501.05092.
- [11] C. Lorcé and Q.-T. Song, Phys. Lett. B **843**, 138016 (2023), 2303.11538.
- [12] M. V. Polyakov, Phys. Lett. B **555**, 57 (2003), hep-ph/0210165.
- [13] M. Burkardt, Phys. Rev. D **62**, 071503 (2000), [Erratum: Phys.Rev.D 66, 119903 (2002)], hep-ph/0005108.
- [14] M. Burkardt, Int. J. Mod. Phys. A **18**, 173 (2003), hep-ph/0207047.
- [15] G. A. Miller, Phys. Rev. Lett. **99**, 112001 (2007), 0705.2409.
- [16] G. A. Miller, Ann. Rev. Nucl. Part. Sci. **60**, 1 (2010), 1002.0355.
- [17] C. Lorcé, H. Moutarde, and A. P. Trawiński, Eur. Phys. J. C **79**, 89 (2019), 1810.09837.
- [18] A. Freese and G. A. Miller, Phys. Rev. D **103**, 094023 (2021), 2102.01683.
- [19] C. E. Carlson and M. Vanderhaeghen, Phys. Rev. Lett. **100**, 032004 (2008), 0710.0835.
- [20] Z. Abidin and C. E. Carlson, Phys. Rev. D **78**, 071502 (2008), 0808.3097.
- [21] C. Lorcé, Phys. Rev. Lett. **125**, 232002 (2020), 2007.05318.
- [22] C. Lorcé and P. Wang, Phys. Rev. D **105**, 096032 (2022), 2204.01465.
- [23] Y. Chen and C. Lorcé, Phys. Rev. D **106**, 116024 (2022), 2210.02908.
- [24] E. Leader and C. Lorcé, Phys. Rept. **541**, 163 (2014), 1309.4235.
- [25] B. L. G. Bakker, E. Leader, and T. L. Trueman, Phys. Rev. D **70**, 114001 (2004), hep-ph/0406139.
- [26] C. Lorcé, L. Mantovani, and B. Pasquini, Phys. Lett. B **776**, 38 (2018), 1704.08557.
- [27] J. C. Collins, A. Duncan, and S. D. Joglekar, Phys. Rev. D **16**, 438 (1977).
- [28] O. V. Teryaev (1999), hep-ph/9904376.
- [29] P. Lowdon, K. Y.-J. Chiu, and S. J. Brodsky, Phys. Lett. B **774**, 1 (2017), 1707.06313.
- [30] S. Cotogno, C. Lorcé, and P. Lowdon, Phys. Rev. D **100**, 045003 (2019), 1905.11969.
- [31] I. A. Perevalova, M. V. Polyakov, and P. Schweitzer, Phys. Rev. D **94**, 054024 (2016), 1607.07008.
- [32] C. Lorcé and P. Schweitzer (2025), 2501.04622.
- [33] K. Goeke, J. Grabis, J. Ossmann, M. V. Polyakov, P. Schweitzer, A. Silva, and D. Urbano, Phys. Rev. D **75**, 094021 (2007), hep-ph/0702030.
- [34] H.-Y. Won, H.-C. Kim, and J.-Y. Kim, Phys. Lett. B **850**, 138489 (2024), 2302.02974.
- [35] H.-Y. Won, J.-Y. Kim, and H.-C. Kim, Phys. Rev. D **106**, 114009 (2022), 2210.03320.
- [36] H.-Y. Won, H.-C. Kim, and J.-Y. Kim, Phys. Rev. D **108**, 094018 (2023), 2307.00740.
- [37] H.-Y. Won, H.-C. Kim, and J.-Y. Kim, JHEP **05**, 173 (2024), 2310.04670.
- [38] C. Lorcé, Eur. Phys. J. C **78**, 785 (2018), 1805.05284.
- [39] J.-Y. Kim and H.-C. Kim, Phys. Rev. D **104**, 074003 (2021), 2106.10986.
- [40] J.-Y. Kim, B.-D. Sun, D. Fu, and H.-C. Kim, Phys. Rev. D **107**, 054007 (2023), 2208.01240.
- [41] Y. Chen and C. Lorcé, Phys. Rev. D **107**, 096003 (2023), 2302.04672.
- [42] K.-H. Hong, J.-Y. Kim, and H.-C. Kim, Phys. Rev. D **107**, 074004 (2023), 2301.09267.
- [43] Y. Chen, Y. Li, C. Lorcé, and Q. Wang, Phys. Rev. D **110**, L091503 (2024), 2405.12943.
- [44] Y. Chen (2024), 2411.12521.
- [45] M. Jacob and G. C. Wick, Annals Phys. **7**, 404 (1959).

EF longitudinal momentum distributions for an unpolarized nucleon

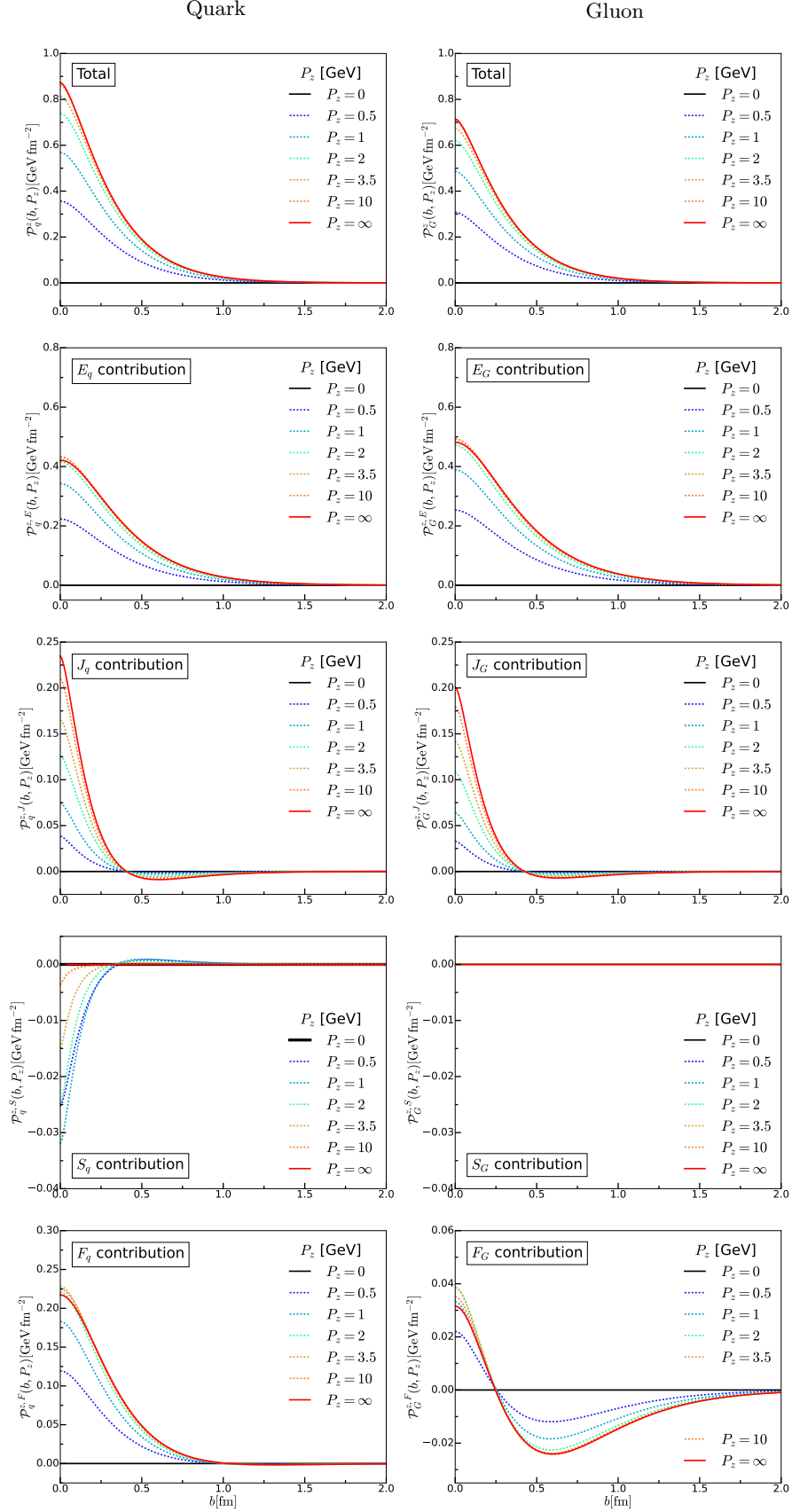


FIG. 8: Radial EF distributions of longitudinal momentum in an unpolarized nucleon for different values of the nucleon momentum. The total longitudinal momentum distribution is normalized to  $M\beta_P$ . The left (right) column corresponds to the quark (gluon) contribution. The first row depicts the sum of the four contributions shown in the other rows. Based on the simple multipole model of Ref. [17] for the EMT FFs.

EF longitudinal thrust distributions for the unpolarized nucleon

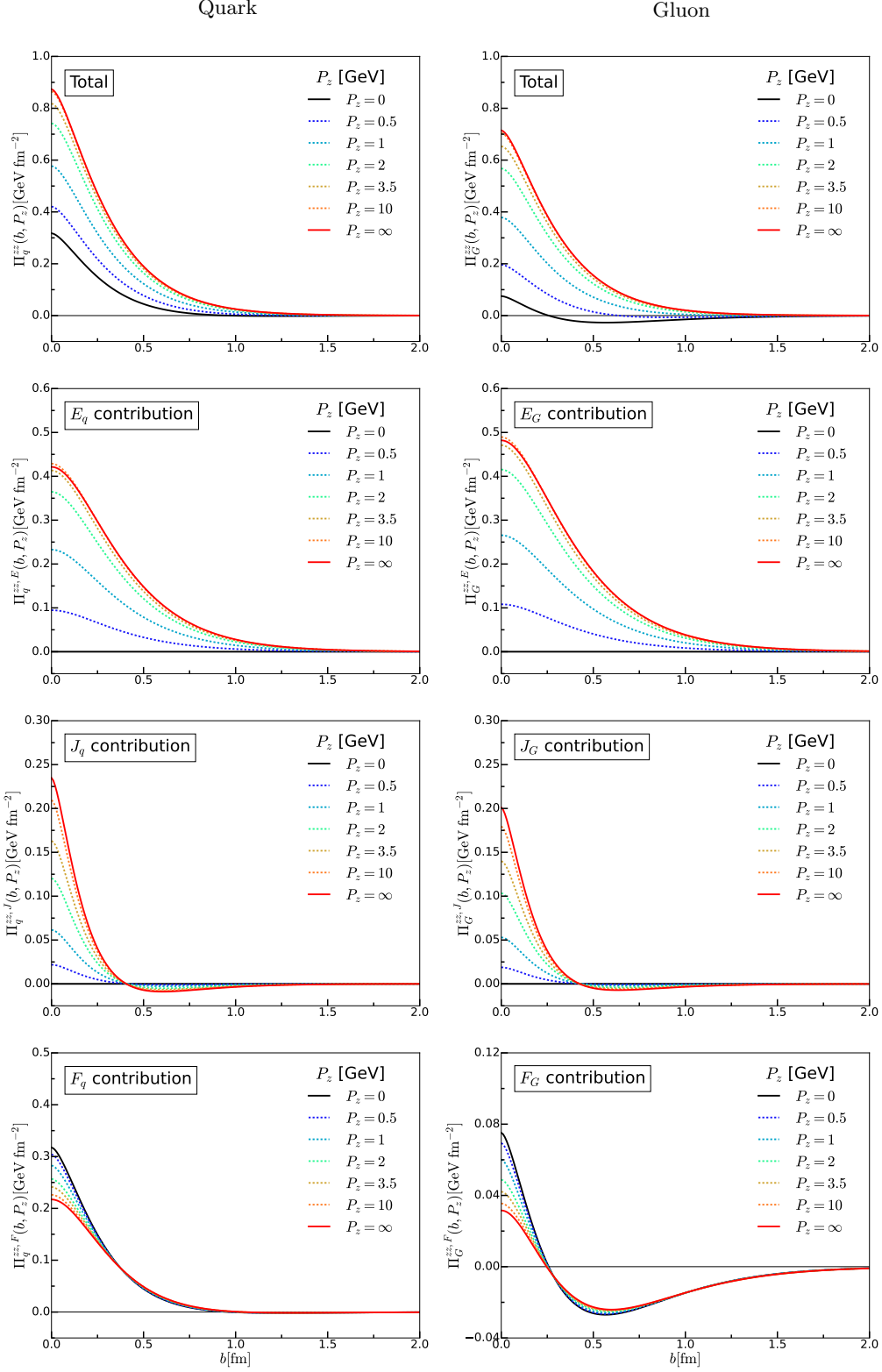


FIG. 9: Radial EF distributions of longitudinal thrust in an unpolarized nucleon for different values of the nucleon momentum. The total longitudinal thrust distribution is normalized to  $M\beta_P^2$ . The left (right) column corresponds to the quark (gluon) contribution. The first row depicts the sum of the three contributions shown in the other rows. Based on the simple multipole model of Ref. [17] for the EMT FFs.

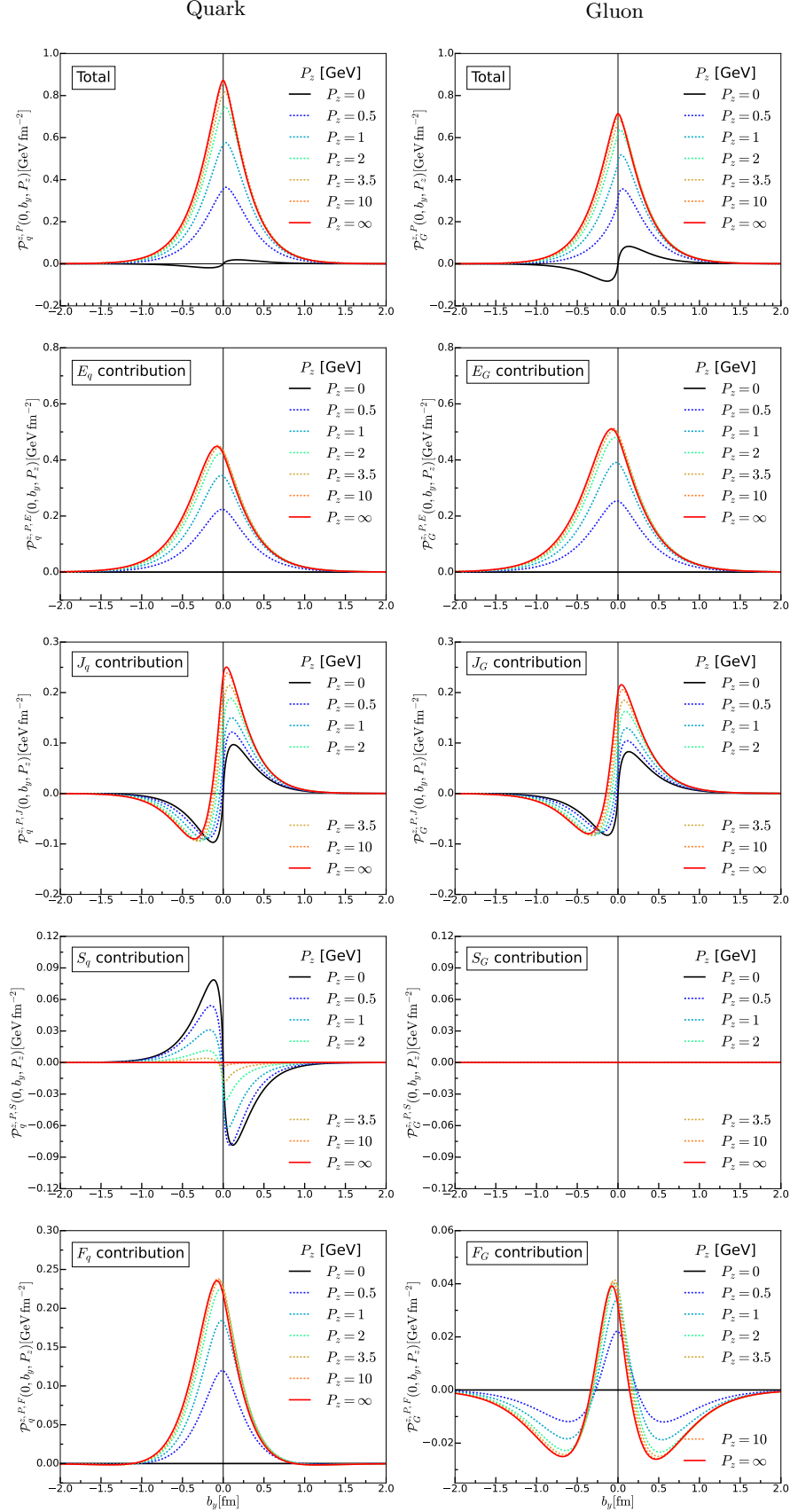
**EF longitudinal momentum distributions for a transversely polarized nucleon**


FIG. 10: EF distributions of longitudinal momentum at  $b_x = 0$  in a nucleon polarized along the  $x$ -axis for different values of the nucleon momentum. The total longitudinal momentum distribution is normalized to  $M\beta_P$ . The left (right) column corresponds to the quark (gluon) contribution. The first row depicts the sum of the four contributions shown in the other rows. Based on the simple multipole model of Ref. [17] for the EMT FFs.

EF longitudinal thrust distributions for the transversely polarized nucleon

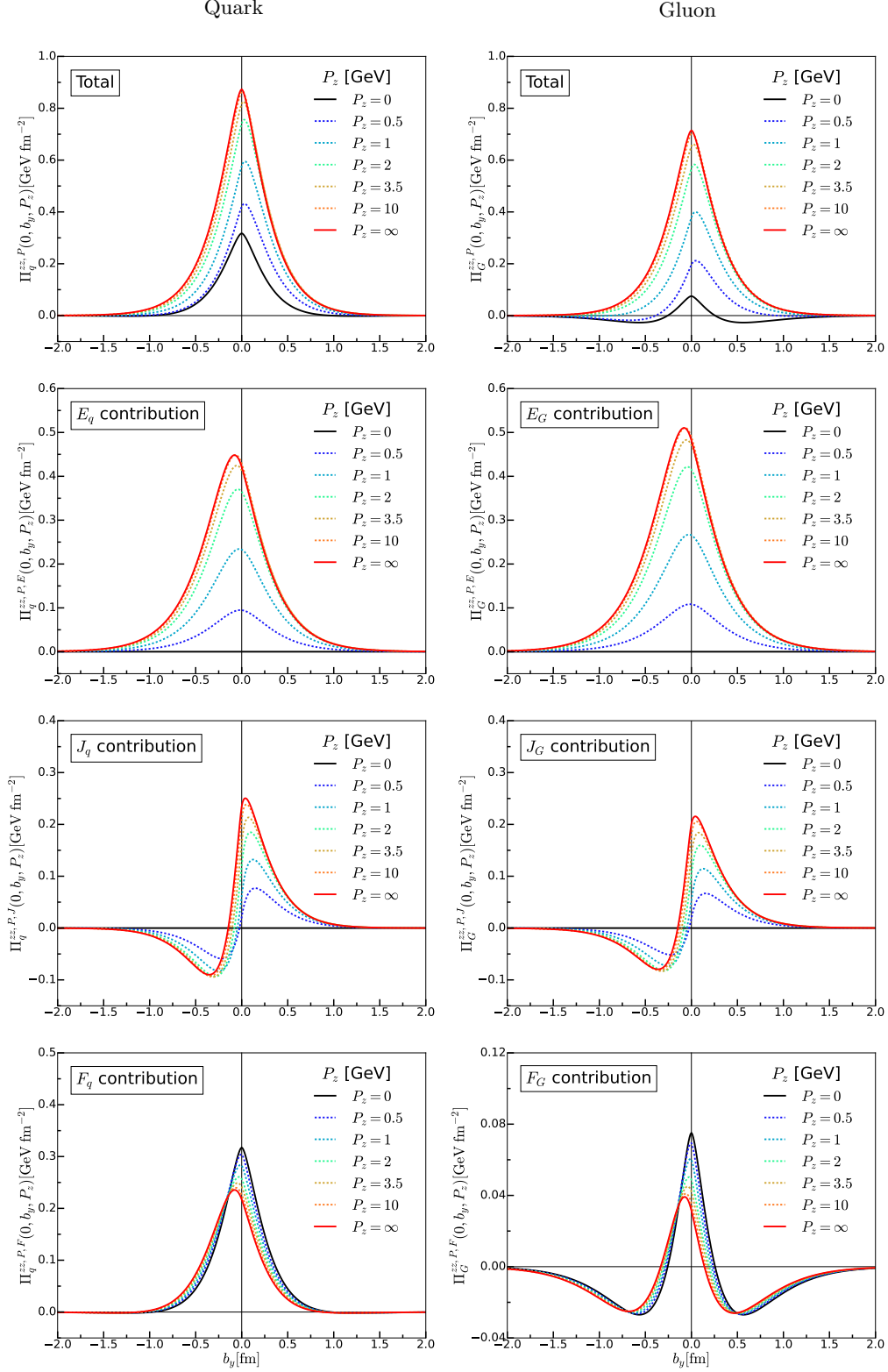


FIG. 11: EF distributions of longitudinal thrust at  $b_x = 0$  in a nucleon polarized along the  $x$ -axis for different values of the nucleon momentum. The total longitudinal thrust distribution is normalized to  $M\beta_p^2$ . The left (right) column corresponds to the quark (gluon) contribution. The first row depicts the sum of the three contributions shown in the other rows. Based on the simple multipole model of Ref. [17] for the EMT FFs.

- [46] L. Durand, P. C. DeCelles, and R. B. Marr, *Phys. Rev.* **126**, 1882 (1962).
- [47] C. Lorcé, *Phys. Rev. D* **97**, 016005 (2018), 1705.08370.
- [48] H.-Y. Won and C. Lorcé, in preparation (2024).
- [49] C. Lorcé, *Eur. Phys. J. C* **81**, 413 (2021), 2103.10100.
- [50] P. A. M. Dirac, *Rev. Mod. Phys.* **21**, 392 (1949).
- [51] S. J. Brodsky, H.-C. Pauli, and S. S. Pinsky, *Phys. Rept.* **301**, 299 (1998), hep-ph/9705477.
- [52] V. Lyubushkin et al. (NOMAD), *Eur. Phys. J. C* **63**, 355 (2009), 0812.4543.
- [53] A. A. Aguilar-Arevalo et al. (MiniBooNE), *Phys. Rev. D* **82**, 092005 (2010), 1007.4730.
- [54] L. Fields et al. (MINERvA), *Phys. Rev. Lett.* **111**, 022501 (2013), 1305.2234.
- [55] G. A. Fiorentini et al. (MINERvA), *Phys. Rev. Lett.* **111**, 022502 (2013), 1305.2243.
- [56] P. Adamson et al. (MINOS), *Phys. Rev. D* **91**, 012005 (2015), 1410.8613.
- [57] K. Abe et al. (T2K), *Phys. Rev. D* **92**, 112003 (2015), 1411.6264.
- [58] K. Abe et al. (T2K), *Phys. Rev. D* **93**, 112012 (2016), 1602.03652.
- [59] K. Kim, H. Gil, and C. H. Hyun, *Phys. Lett. B* **833**, 137273 (2022), 2203.16841.
- [60] A. V. Butkevich and S. V. Luchuk, *Phys. Rev. D* **99**, 093001 (2019), 1812.11073.
- [61] J. E. Amaro and E. Ruiz Arriola, *Phys. Rev. D* **93**, 053002 (2016), 1510.07532.
- [62] A. Liesenfeld et al. (A1), *Phys. Lett. B* **468**, 20 (1999), nucl-ex/9911003.
- [63] R. Gonzalez-Jimenez, M. V. Ivanov, M. B. Barbaro, J. A. Caballero, and J. M. Udias, *Phys. Lett. B* **718**, 1471 (2013), 1210.6344.
- [64] J. Nieves, I. Ruiz Simo, and M. J. Vicente Vacas, *Phys. Rev. C* **83**, 045501 (2011), 1102.2777.
- [65] C. Alexandrou et al., *Phys. Rev. D* **103**, 034509 (2021), 2011.13342.
- [66] R. S. Sufian, K.-F. Liu, and D. G. Richards, *JHEP* **01**, 136 (2020), 1809.03509.
- [67] R. Gupta, Y.-C. Jang, H.-W. Lin, B. Yoon, and T. Bhattacharya, *Phys. Rev. D* **96**, 114503 (2017), 1705.06834.
- [68] C. Alexandrou, M. Constantinou, K. Hadjiyiannakou, K. Jansen, C. Kallidonis, G. Koutsou, and A. Vaquero Aviles-Casco, *Phys. Rev. D* **96**, 054507 (2017), 1705.03399.
- [69] C. Alexandrou, M. Brinet, J. Carbonell, M. Constantinou, P. A. Harraud, P. Guichon, K. Jansen, T. Korzec, and M. Papinutto (ETM), *Phys. Rev. D* **83**, 045010 (2011), 1012.0857.
- [70] C. Alexandrou, G. Koutsou, T. Leontiou, J. W. Negele, and A. Tsapalis, *Phys. Rev. D* **76**, 094511 (2007), [Erratum: *Phys.Rev.D* 80, 099901 (2009)], 0706.3011.
- [71] V. Bernard, L. Elouadrhiri, and U.-G. Meissner, *J. Phys. G* **28**, R1 (2002), hep-ph/0107088.
- [72] C. Lorcé, B. Pasquini, X. Xiong, and F. Yuan, *Phys. Rev. D* **85**, 114006 (2012), 1111.4827.